Novel CuI coordination polymer self-assembled from 2,5-bis(pyridin-4-yl)-1,3,4-oxadiazole and thiocyanate ions: Synthesis, structural characterization, Hirshfeld surface analysis, thermal and magnetic studies

Abdelhakim Laachir, Ferdaousse Rhoufal, Salaheddine Guesmi, El Mostafa Ketatni, Mohamed Saadi, Lahcen El Ammari, Olivier Mentré, Fouad Bentiss

Novel Cu^{I} coordination polymer self-assembled from 2,5-bis(pyridin-4-yl)-1,3,4-oxadiazole and thiocyanate ions: Synthesis, structural characterization, Hirshfeld surface analysis, thermal and magnetic studies

Abdelhakim Laachir[a], Ferdaousse Rhoufal[a], Salaheddine Guesmi[a], El Mostafa Ketatni[b], Mohamed Saadi[c], Lahcen El Ammari[c], Olivier Mentré[d], Fouad Bentiss[e,*]

[a] Laboratory of Coordination and Analytical Chemistry (LCCA), Faculty of Sciences, Chouaib Doukkali University, PO Box 20, M-24000 El Jadida, Morocco
[b] Laboratory of Molecular Chemistry, Materials and Catalysis, Faculty of Sciences and Technics, Sultan Moulay Slimane University, PO Box 523, M-23000 Beni-Mellal, Morocco
[c] Laboratoire de Chimie Appliquée des Matériaux, Centre des Sciences des Matériaux, Faculty of Science, Mohammed V University in Rabat, Avenue Ibn Batouta, B.P. 1014, Rabat, Morocco
[d] Univ. Lille, CNRS, Centrale Lille, UMR 8181, - UCCS - Unité de Catalyse et de Chimie du Solide, F-59000 Lille, France
[e] Laboratory of Catalysis and Corrosion of Materials (LCCM), Faculty of Sciences, Chouaib Doukkali University, PO Box 20, M-24000 El Jadida, Morocco

ARTICLE INFO

Article history:
Received 23 May 2022
Revised 2 July 2022
Accepted 22 July 2022
Available online 23 July 2022

Keywords:
2,5-Bis(pyridin-2-yl)-1,3,4-oxadiazole
Thiocyanate
Coordination polymer Cu^{I}
Crystal structure
Hirshfeld surface analysis
Magnetic properties

ABSTRACT

The synthesis and crystal structure of one-dimensional (1-D) coordination polymer from an angular dipyridyl ligand 2,5-bis(pyridine-4-yl)-1,3,4-oxadiazole (4-pox) and $CuCl_2 \cdot 2H_2O$, $[Cu^{I}(4\text{-poxH})(SCN)(\mu_{1,3}\text{-SCN})]_n$ (named complex **1**), are reported. The investigated copper(I) complex crystallizes in the monoclinic crystal system with space group $P2_1/n$. UV–vis and FTIR suggest the co-presence of the 4-pox ligand and the pseudohalide, in the isolated complex. This was confirmed by a crystallographic study which shows that the copper is in a tetrahedral environment, linked to two thiocyanate groups and to two nitrogen atoms, one belonging to the pyridine ring and the others to thiocyanate group. The crystallographic study also reveals the protonation of the unbound organic ligand pyridine. The crystal cohesion is assured by different intermolecular hydrogen bonds, $\pi-\pi$ stacking, and coordination bonds (N–Cu and S–Cu). Therefore, the one-dimensional coordination chains are further interconnected by hydrogen bonds and $\pi-\pi$ stacking to from a three-dimensional supramolecular framework. This behaviour was confirmed by Hirshfeld surface analysis. The thermal analysis reveals that complex **1** is thermally stable up to 160 °C. The magnetic measurements indicated the diamagnetic nature of this Cu^{I} coordination polymer.

1. Introduction

In recent decades the synthesis of coordination complexes and polymers based on N-heterocyclic ligands has undergone rapid development for their different potential activities in various fields as electrochemistry [1–3], energy storage [1,2], catalysis [4–6], photoreaction [7–9] and photo-catalysis [3], as well as magnetism [10–12]. Other polymers can also be used as potential adsorbents of heavy metal from polluted water and thus contribute to environment protection [13]. The engineering coordination often used for the synthesis of these supramolecular entities, more particularly copper complexes, is the so-called self-assembly method, realised in one step, between a metal salt and an organic ligand with or without coligand [5,14-16]. In addition, the aforementioned complexes of different dimensions and topologies are used in specific reactions such as photo-controlled cyclization reactions [8,9], or catalytic oxidation of alcohols to aldehydes [5]. The same type of reaction is carried out by the metalloenzyme Galactose Oxidase, a copper-based complex that catalyses the oxidation of D-galactose (primaryalcohol) to D-galactohexdialdose (aldehyde) in the presence of dioxygen, via a mechanism where the ligands are redox-active and the metal, as active site, is reduced to Cu(I) during the catalytic cycle [17–19].

The coordination chemistry of N-heterocyclic ligands, such as, thiadiazoles and oxadiazoles, is an emerging and rapidly developing area of research. This mainly comes down to their potential applications in different fields such as biology [20,21], catalysis [22] and magnetism [23]. Indeed, thiadiazole and oxadiazole

* Corresponding author.
E-mail address: fbentiss@gmail.com (F. Bentiss).

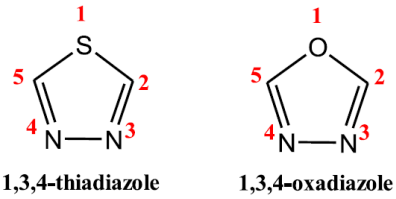

Fig. 1. Numbering of the 1,3,4-thiadiazole and 1,3,4-oxadiazole rings systems.

are prevalent and important five-membered heterocyclic systems containing two nitrogen atoms and a sulfur or oxygen atom. There are several isomers in the literature but the most used are 1,3,4-thiadiazole and 1,3,4-oxadiazole (Fig. 1). They are very weak bases due to the inductive effect of the sulfur/oxygen atom and possess relatively high aromaticity, we also note that when the 2 or 5 positions of these entities are substituted, they readily react with transition metals and lead to coordination compounds potentially applicable in various fields [24–26]. In point of fact, we were able to synthesize several complexes and coordination polymers based on *N*-heterocyclic ligands in particular 2,5-bis(pyridin-2-yl)−1,3,4-oxadiazole (2-pox), 2,5-bis(pyridin-2-yl)−1,3,4-thiadiazole (2-pth) and 2,5-bis(pyridin-4-yl)−1,3,4-oxadiazole (4-pox) (Fig. 2). The detailed study of the latters showed an antifungal and antimicrobial activity in some cases and magnetic properties in others [27,28].

On the other hand, during the last decades the development of coordination polymers from organic ligands and pseudohalides has been the subject of great interest. Actually, their uses as co-ligands with a heterocyclic compound can lead to the formation of potentially interesting materials in the biological and magnetic fields [10,29,30]. The pseudohalide that we have used recently in our research is the thiocyanate anion. We chose the SCN^- ion because it is a versatile ligand that can bind to transition metals in different modes (Fig. S1), thus forming several types of complexes: monomers, dimers or coordination polymers with different dimensions and topologies [31–33]. Indeed, the choice is justified by the different applications of thiocyanate complexes in various fields [34–37]. With transition metal salts in the presence of 2,5-bis(pyridin-2-yl)−1,3,4-oxadiazole (2-pox) or 2,5-bis(pyridin-2-yl)−1,3,4-thiadiazole (2-pth) and SCN^- ions, we generally obtained mono or binuclear complexes [38–40]. However, the use of $CuCl_2{\cdot}2H_2O$ as transition metal salt recently allowed the synthesis an unusual mixed-valence Cu^{II}/Cu^{I} coordination polymer, $[Cu^{I}_3Cu^{II}(2\text{-pth})_2(SCN)_5]_n$, based on 2-pth as ligand and thiocyanate as coligand [16]. The latter is the product of a partial reduction of Cu^{II} to Cu^{I} by the presence of thiocyanate in acetonitrile/water solution. This copper complex shows a paramagnetic behaviour and significant antibacterial activity against the phytopathogenic bacteria *Agrobacterium tumefaciens*. However, with the angular dipyridyl ligand 2,5-bis(pyridin-4-yl)−1,3,4-oxadiazole (4-pox) and thiocyanate ion, different mononuclear complexes of general formula $[M^{II}(4\text{-pox})_2(NCS)_2(H_2O)_2]$ were described, where M = Fe^{II}, Co^{II}, Mn^{II}, Cd^{II}, and Ni^{II}, and revealed an octahedral geometry around the metal site with pseudohalide and organic ligands in mutually trans positions [41–44]. Also, the crystal structure results indicated that such mononuclear structure is thermodynamically stable and independent to the type of the metal(II) ions [44]. On the other hand, a family of mercury(II)–organic polymeric complexes, generated from 4-pox ligand, with the formula $[Hg(4\text{-pox})_n X_2]$ where X = SCN^-, I^-, Br^-, NO_2^- and N_3^-, has been reported and showed the influence of the counter-ions on the coordination mode of the 4-pox ligand in mercury(II) coordination polymers [45]. Hydrothermal reaction of CuCN with 4-pox yielded copper (I) coordination polymer $[Cu^{I}(CN)(4\text{-pox})]_n$ involving 2-D structure [46]. This complex showed blue fluorescent emission and the luminescent mechanism was assigned to metal-to-ligand charge transfer (MLCT) where the electron is transferred from Cu(I) to cyanide group. Fang et al. described the formation of $[Cu^{I}_3(4\text{-pox})I_3]_n$ in situ metal/ligand solvothermal reaction of CuI and 4-pox, that showed 3-D complicated MOFs consisting of a three-stranded helical chains and the double-stranded $[CuI]_n$ chains [47]. This copper (I) coordination complex is nonluminescent and showed a broad absorption band covering the whole UV–vis-NIR spectrum range.

As a continuation of our work, we describe, in this contribution, the synthesis and structural characterization of a novel Cu^{I} coordination polymer, noted $[Cu^{I}(4\text{-poxH})(SCN)(\mu_{1,3}\text{-SCN})]_n$ (complex **1**), based on 2,5-bis(pyridin-4-yl)−1,3,4-oxadiazole (4-pox) as ligand and the thiocyanate anion as coligand, which is assembled into 3-D extended network via intermolecular hydrogen bonds and $\pi-\pi$ stacking interactions. Hirshfeld surface analysis, spectroscopic characterizations (FTIR, UV–Visible) as well as thermal study on complex **1** are carried out. The magnetic measurements are also performed and discussed.

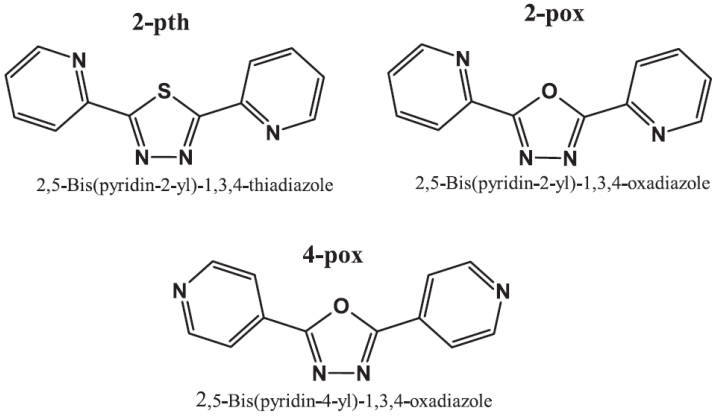

Fig. 2. Example of *N*-heterocyclic ligands.

2. Experimental

2.1. Materials and methods

All chemicals for synthesis were obtained from commercial sources and used as received. Water used in the syntheses was doubly distilled. The ligand, namely 2,5-bis(pyridin-4-yl)−1,3,4-oxadiazole (4-pox), was synthesized according to the literature procedure [48] and the characterization detail of 4-pox is given in supporting information.

An appropriate single crystal of complex **1** was carefully selected using a polarizing microscope for X-ray data collection, at room temperature, using Bruker D8 Venture Super DUO diffractometer with PHOTON100 CMOS area-detector and monochromatic Mo$K\alpha$ radiation (λ = 0.71073 Å). APEX3 software was used for data collection [49] and the absorption correction was performed by multi-scan semi-empirical method using SADABS [50]. The crystal structure was solved by the direct method and refined by weighted full matrix least-square on F^2 techniques using the programs SHELXT 2014 [51] and SHELXL 2018 [52] incorporated in WinGX program [53]. For the structural drawing, MERCURY software was used [54]. Non hydrogen atoms were refined with anisotropic thermal parameters. The C-bound H atoms were geometrically placed (C–H = 0.93 - 0.98 Å) and refined as riding with U_{iso}(H) = 1.2 - 1.5 U_{eq}(C). The O-bound H atom was located in a difference Fourier map and refined freely.

Routine powder X-ray diffraction (PXRD) data of complex **1** phase have been collected at room temperature in the angular range 5 to 85 of 2θ with a scan step width 0.016° using a X'pert Pro-PANalytical $\theta/2\theta$ diffractometer (CuKα radiation, λ = 1.5405 Å) in Bragg-Brentano geometry. Cell parameters have been refined using refined using the "*pattern matching*" option of Fullprof suite [55,56], by means of PXRD profile patterns adjustment.

Fourier Transform InfraRed (FTIR) spectra were recorded on a SHIMADZU FT-IR 8400S spectrometer with a Smart iTR attachment and diamond attenuated total reflectance (ATR) crystal in the range 400–4000 cm^1. Ultraviolet-visible (UV–Visible) absorption spectra in DMF solvent were recorded in the range 200–900 nm using a SHIMADZU 2450 spectrophotometer. Element analyses (C, H, N and S) were performed on a VARIO-ELEMENTAR analyser. The ^{1}H and ^{13}C NMR spectra of 4-pox were recorded with the Bruker AVANCE 300 at 25 °C. All chemical shifts ^{1}H and ^{13}C are given in ppm using dimethyl sulfoxide-d_6 (DMSO–d_6) as solvent.

Thermogravimetric analysis (TGA) was carried out on a SDT-Q600 thermal analyser and alumina crucibles, in the range of room temperature to 800 °C under air flow (99 ml/min) with 5 °C min^{-1} fixed heating rate. The TGA curve has been normalized with respect to the sample weight.

Magnetic measurements (thermal dependence of the susceptibility and field dependence of the magnetization) have been collected using the VSM module of a Physical Property Measurement System (PPMS) Dynacool, maximum field = 9T.

2.2. General synthetic procedure for complex 1

To a solution of KSCN (0.4 mmol, 40 mg) in 20 mL of acetone, $CuCl_2 \cdot 2H_2O$ (0.2 mmol, 34 mg) was added under magnetic stirring. The colour turns red immediately and after 10 min, the solution was filtered and added to a solution of 4-pox (0.1 mmol, 22 mg) dissolved beforehand in 20 ml of acetone. The mixture was refluxed for one hour under magnetic stirring and was filtered while hot. The filtrate was kept at room temperature and after one-week blocks of crystals were obtained. They were separated, washed with cold ethanol, dried under vacuum and used as isolated for single crystal X-ray analysis. Yield: 45% (based on Cu). Anal. Calcd. (%) for $C_{14}H_9CuN_6OS_2$: C, 41.53; H, 2.24; N, 20.75; S, 15.83. Found (%): C, 41.62; H, 1.97; N, 20.79; S, 15.81; IR-ATR (cm^{-1}): 3045 (w), 2073 (vs), 1614 (m), 1569 (w), 1478–1564 (s), 1414 (m), 1243 (m), 1062 (w), 994 (m), 823 (s), 703 (vs), 496 (s), 457(w); UV–Vis (λ_{max}, nm (ε_{max}, M^{-1} cm^{-1})) in DMF solvent: 287 (14400), 271 (22500).

2.4. Hirshfeld surface analysis

Hirshfeld surface of complex **1** was analysed in order to explore the nature of different types of intermolecular interactions in the crystal packing motifs. Thus, a Hirshfeld surface analysis [57] and the associated two-dimensional fingerprint plots [58] were performed using CrystalExplorer17.5 [59] to figure out the normalized contact distance (d_{norm}), which depends on contact distances to the closest atoms outside (d_e) and inside (d_i) the surface. The 3D d_{norm} surfaces are mapped over a fixed colour scale of −0.6930 to 1.0944 for complex **1**, and shape index mapped in the colour range of −1.0 to 1.0 a.u. The HS mapped over the electrostatic potential was generated using TONTO program [60] integrated in CrystalExplorer with STO-3 G basis set at the Hartree-Fock level of theory energy in the range −0.1726 to 0.2954 a.u for complex molecule.

3. Results and discussion

3.1. Synthesis and general characterizations

3.1.1. Synthesis detail

The title complex was prepared from reaction of the 4-pox ligand and SCN^- with copper(II) chloride dihydrate. The obtained complex is the result of the reduction of Cu^{II} to Cu^{I} in acetone solution, the protonation of a single pyridine ring of 4-pox ligand and the copper coordination with two thiocyanate ions. The reduction of the copper could be explained by the presence of thiocyanate ions in the reaction medium which could lead to the $Cu(NCS)_2$ derivative, which is unstable in solution and would lead to the monovalent CuSCN complex and $(SCN)_2$ [61,62]. The latter decomposes in aqueous medium with the formation of HNCS, H_2SO_4, and HCN, as degradation products that could protonate 4-pox ligand. Such protonation was observed previously in the case of 2,5-bis(pyridin-2-yl)−1,3,4-thiadiazole (2-pth) [63], as the result of the proton donor-acceptor reaction between perchloric acid and a single pyridine of the organic ligand.

3.1.2. UV-visible study

Characterization of the 4-pox ligand and complex **1** was performed by UV-visible absorption spectroscopy in DMF at room temperature and the obtained electronic spectra are shown in Fig. S2. The absorption maxima with the corresponding extinction coefficients of both compounds are given in Table S1. The UV–vis spectrum of the Cu^{I} complex shows two intense bands in the UV range at 287 and 271 nm attributable to intra-ligand electronic transitions $n \rightarrow \pi^*$ and $\pi \rightarrow \pi^*$ respectively (Fig. S2). The same transitions for the free 4-pox ligand have the same shape as those of the complex, at 282 and 266 nm, thus confirming the presence of heterocyclic ligand in the Cu^{I} polymeric complex.

3.1.3. FTIR spectroscopy

The FTIR spectra of the 4-pox ligand and its copper (I) complex are illustrated in

Fig. S3 and the corresponding data are given in Table S2. Compared to 4-pox ligand, the infrared spectrum of complex **1** is distinguished mainly by the appearance of a new intense absorption band located towards 2073 cm^{-1} which correspond to the vibration ν(CN) of the thiocyanate group. This value is comparable to similar complexes cited in the literature [63–65]. The FTIR spectrum also reveals the presence of characteristic bands

Table 1
Crystal data, data collection and structure refinement details of complex **1**.

Crystal data	
Chemical formula	$C_{14}H_9CuN_6OS_2$
M_r (g mol^{-1})	404.93
Crystal system, space group	Monoclinic, $P2_1/n$
Temperature (K)	296
a, b, c (Å)	5.9175 (4), 14.6841 (11), 18.4048 (13)
β (°)	94.431 (3)
V (Å^3)	1594.5 (2)
Z	4
Radiation type	Mo $K\alpha$
μ (mm^{-1})	1.65
Crystal size (mm)	0.34 × 0.15 × 0.14
Data collection	
Diffractometer	Bruker D8 VENTURE Super DUO
Absorption correction	Multi-scan *SADABS*(Krause et al., 2015)
T_{min}, T_{max}	0.638, 0.746
No. of measured, independent and observed [$I > 2\sigma(I)$] reflections	74,237, 4113, 3470
R_{int}	0.044
(sin $\theta/\lambda)_{max}$ (Å^{-1})	0.676
Refinement	
$R[F^2 > 2\sigma(F^2)]$, $wR(F^2)$, S	0.033, 0.086, 1.07
No. of reflections	4113
No. of parameters	217
H-atom treatment	H-atom parameters constrained
$\Delta\rho_{max}$, $\Delta\rho_{min}$ (e Å^{-3})	0.38, −0.49

Table 2
Hydrogen-bond geometry (Å, °) for complex **1**.

D–H···*A*	*D*–H	H···*A*	*D*···*A*	*D*–H···*A*
N4–H4N···N5^{i}	0.86	1.88	2.705 (3)	161
C2–H2···N2^{ii}	0.93	2.53	3.351 (3)	147
C11–H11···S1^{iii}	0.93	2.64	3.462 (3)	147

Symmetry codes: (i) x-3/2, -y + 1/2, z-1/2; (ii) -x + 1, -y + 1, -z + 1; (iii) -x-1/2, y-1/2, -z + 3/2.

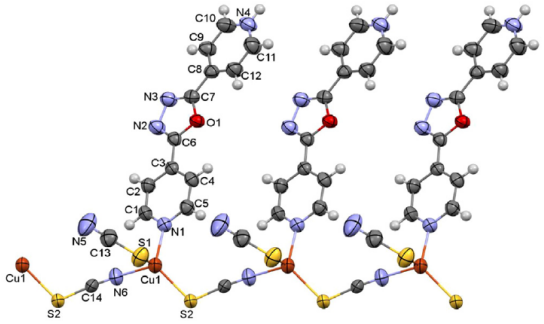

Fig. 3. The molecular structure of complex 1 with displacement ellipsoids drawn at the 50% probability level, building one-dimensional (1-D) coordination polymer along a-axis.

of 4-pox ligand at 3045, 1614, 1569, 1478–1564, 1062 and 994 cm^{-1} corresponding respectively to the vibrations υ(C–H)$_{pyridyl}$, υ(C = N)$_{oxadiazole}$, ν(C = N)$_{pyridyl}$, υ(C = C)$_{pyridyl}$, υ(N–N)$_{oxadiazole}$ and υ(C–O–C)$_{oxadiazole}$. A low intensity absorption band located at 457 cm^{-1} is assigned to the Cu–N bond [65]. These spectroscopic data results allowed us to suggest the presence of the thiocyanate anion and organic ligand in the investigated copper (I) complex.

3.1.4. Thermal study

In order to evaluate the thermal stability of complex **1**, the thermogravimetric analysis (TGA) was carried out under air between 30 and 800 °C. As shown in Fig. S4, the TG curve highlighted mass losses only from 160 °C, indicating that the investigated 1-D coordination polymer is stable in this temperature range, then gradual decomposition occurs essentially in two successive stages between 160 and 640 (69.4% and 6.2% respectively), with a residual mass of 24.4%. Both stages with a total mass loss of 75.6% are attributed to decomposition of organic ligand (4-poxH$^+$) and thiocyanate ion of the copper complex. The first weight loss (observed 69.4%; calcd. 69.9%), between 160 and 360 °C, would correspond to the release of the 4-poxHSCN molecule from the complex **1**. While the second mass loss (observed 6.2%; calcd. 6.4%),%), between 360 and 640 °C, can be attributed to the degradation of the remaining CuSCN entity and the formation of CuS as the residual product (observed 24.4%; calcd. 23.6%).

3.2. Crystal structure description

Details of the crystal structure determination of complex **1** and a summary of the results of its refinement are given in Table 1. Atomic positions, isotropic thermal displacement factors, selected bond lengths and angles are reported in Tables S3-S5 of the additional information file. The hydrogen atoms were positioned in idealized positions and included in the final refinement cycles with isotropic thermal parameters giving the final R_1 = 3.3% and wR_2 = 8.6% for the 4113 unique reflections. Hydrogen bonds are given in Table 2.

The neutral copper(I) complex (complex **1**) crystallizes in the monoclinic symmetry with four formulas pro unit cell. All atoms are in the general position of the space group $P2_1/n$. The asymmetric unit of the crystal structure belonging to this Cu^{I} complex is represented in Fig. 3. The three cycles building the organic moieties of this complex are linked together through an 1,3,4-oxadiazole ring to form a type along (0 1 −1). It should be noted that the 4-poxH$^+$ uses only one nitrogen atom acting as monodentate ligand. The pyridine ring connected to copper atom and the 1,3,4-oxadiazole cycle are nearly coplanar, with the maximum deviation from de mean plan of 0.025 (2) Å at C6 atom. The pyridinium ring is slightly inclined with respect to the 1,3,4-oxadiazole ring and the dihedral angle between them is 6.91(11) °. The inorganic moieties result from a copper atom linked to two thiocyanate groups and to two nitrogen atoms, one belonging to the pyridine ring of 4-poxH$^+$ and the other to nitrogen of thiocyanate group. The M–N bond of 4-poxH$^+$ is larger than M–N bond of SCN$^-$ (Table S5). The two SCN$^-$ anions are coordinate to Cu^{I}, one in a monodentate terminal mode (S-bond) and the second in a bidentate coordination mode ($\mu_{1,3}$-SCN). In addition, the two sulfur and the two nitrogen atoms surrounding the Cu^{I} ions form a distorted tetrahedron, Cu–S bond lengths of 2.2713(6) Å and 2.3673(7) Å, Cu–N are of 2.015(2) Å and 2.053(2) Å (Table S5). In the mononuclear complexes with the general formula [M^{II}(4-pox)$_2$(NCS)$_2$(H$_2$O)$_2$] (M^{II} = Fe^{II}, Co^{II}, Mn^{II}, Cd^{II} and Ni^{II}) previously described [41–44], the 4-pox ligand and NCS$^-$ anion act only as monodendate terminal ligands via the nitrogen atoms. However, in the case of [Hg(4-pox)($\mu_{1,3}$-SCN)$_2$]$_n$ complex reported by Mahmoudi & Morsali [45], the two thiocyanate ions are in bridging mode ($\mu_{1,3}$-SCN) between metal sites and the structure of this compound can be considered as a 1-D coordination polymer of mercury(II) [45].

In the crystal structure of complex **1**, the molecules are linked together by CuS_2N_2 tetrahedral which are interconnected via a vertex through a thiocyanate group forming an infinite chain along the a-axis, resulting therefore in a one-dimensional polymer (Fig. 3). Moreover, the molecules are also linked through N4–H4···N5, C2–H2···N2 and C11–H11···S1 hydrogen bonds to form a two-dimensional (2-D) supramolecular complex as shown in Fig. S5. The resulting crystal packing of this complex is displayed in

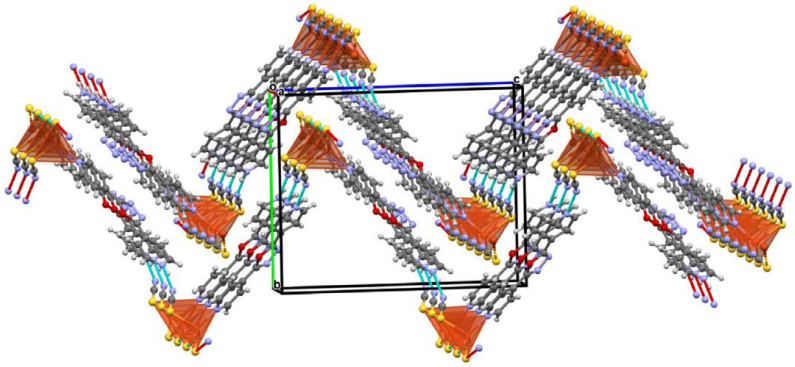

Fig. 4. Three-dimensional (3-D) network of complex 1, showing infinite kinked plan stacking along [0 1 1] direction.

Fig. 4, which shows the molecules building an infinite kinked plan stacking along [0 1 1] direction. In addition, the plans are interconnected by $\pi-\pi$ stacking interactions between the pyridine and 1,3,4-oxadiazole rings, with inter-centroid distance of 3.5549(12) Å as depicted in Fig. 5.

Using powder X-ray diffraction data, the unit cell parameters of copper complex, were refined, as single crystal diffraction, in monoclinic structure, with $P\ 2_1/n$ space group. PXRD refinement was carried out using the pattern matching option of Fullprof program, where only the profile parameters (cell dimensions, symmetry, peak shapes, and zero-point correction) have been refined. Pseudo-Voigt function with an asymmetry correction at low angles was used to describe the peak shape. The angular dependence of the peak full-width at half-max. (H) was described using the following formulation [66]:

$$H = \sqrt{U tan^2\theta + V tan\theta + W} \quad (1)$$

where U, V and W parameters were refined in the process. The final observed, calculated, and difference PXRD patterns resulting from the profile-matching procedure are plotted in Fig. 6. The obtained lattice parameters are: a = 5.9175(3) Å, b = 14.7212(7) Å, c = 18.4143(7) Å, β = 93.685(3) with R_p = 3.22% and R_{wp} = 6.36%. The obtained structure refinement parameters showed that PXRD and crystal diffraction findings are in good agreement indicating that the obtained phase of the coordination polymer is pure.

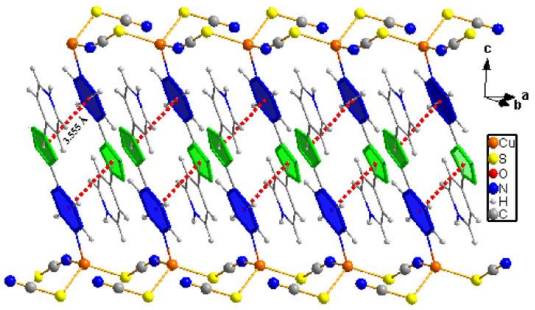

Fig. 5. Crystal packing of complex 1 showing intermolecular $\pi-\pi$ stacking interactions between pyridine and 1,3,4-oxadiazole rings.

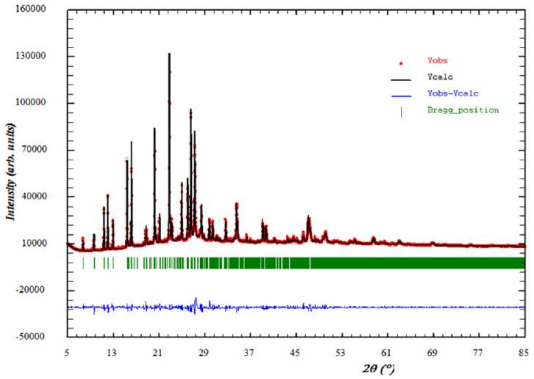

Fig. 6. Results of the profile-matching analysis of complex 1 from the PXRD data. The observed, calculated, and difference patterns are in red, black and blue, respectively. The small marks in green correspond to the Bragg peaks positions. The obtained lattice parameters are: a = 5.9175(3) Å, b = 14.7212(7) Å, c = 18.4143(7) Å, β = 93.685(3) with R_p = 3.22% and R_{wp} = 6.36%.

3.3. Hirshfeld surface analysis

Hirshfeld surface analysis of the investigated copper polymeric complex were generated using high standard surface resolution with the 3D d_{norm}, are shown in Fig. 7a-b and shape-index mapped over the Hirshfeld surface in Fig. 7c. The intense red spots on the Hirshfeld surface mapped with d_{norm} correspond to the N–H···N hydrogen bond, resulting from the interaction between the N-thiocyanate atoms inside the Hirshfeld surface and the hydrogen atoms of pyridine ring outside the surface and vice versa. Other short intermolecular contacts appear as light-red spots, C–H···N/S (Fig. 7a-b). The most closet interactions refer to the Cu–S2 coordination interactions, as they are indicated by the deep red regions on d_{norm} surface, near the metal atoms due to the polymeric nature of Cu complex. The positive and negative electrostatic potential are represented with blue and red surface regions on the Hirshfeld surface mapped over electrostatic potential (Fig. 7d).

As illustrated in Fig. 8, the corresponding fingerprint plots for the investigated copper (I) complex are shown with characteristic pseudo-symmetric wings in the d_e and d_i diagonal axes and those delineated into N···H/H···N, C···H/H···C, H···S/S···H, H···H, C···C, C···N/N···C, and C···S/S···C. The relative contributions of various intermolecular interactions to the Hirshfeld surface area are summa-

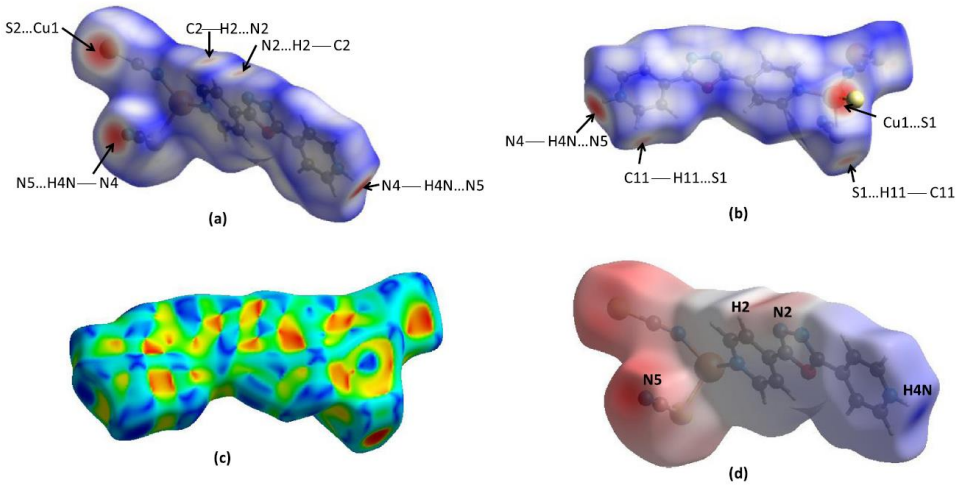

Fig. 7. Views of the Hirshfeld surfaces of complex 1 plotted over (a) and (b) d_{norm}, (c) shape-index map and (d) electrostatic potential.

rized in Table S6. The N···H/H···N (interactions 26.3%), corresponding to N4–H4···N5 and C2–H2···N2 interactions, is represented by the spikes in the bottom right and left region, $d_e + d_i \approx 1.75$ Å (Fig. 8b).

In the absence of weak C–H···π interactions in the crystal, a pair characteristic wings resulting in the fringerprint plot delineated into C···H/H···C contacts, with 17.1% contribution to the Hirshfeld surface, have a symmetrical distribution of points, with the tips at $d_e + d_i \approx 2.75$ Å (Fig. 8c). The smaller red spot in the d_{norm} map show weak S···H/H···S, contacts attributed to C11–H11···S1 hydrogen bonds with notable contribution of 15.8% to the Hirshfeld surface area (Fig. 8d), with the tips at $d_e + d_i \approx 2.55$ Å. The H···H con-

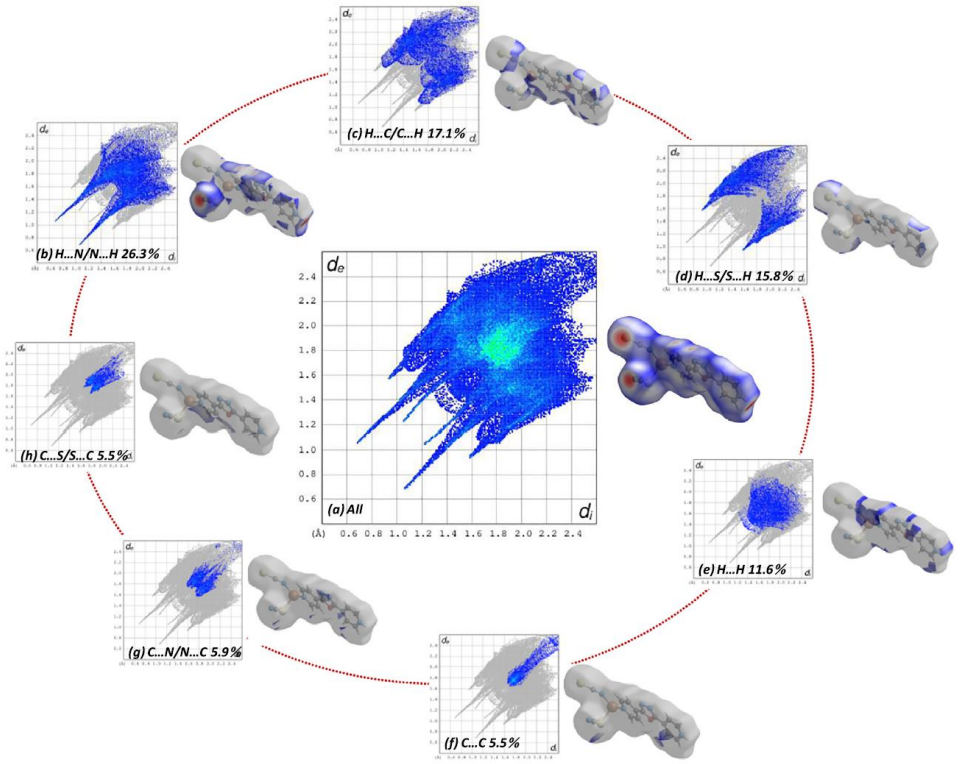

Fig. 8. a) The overall two-dimensional fingerprint plots of complex 1, and those delineated into: b) N···H/H···N, c) C···H/H···C, d) H···S/S···H, e) H···H, f) C···C, g) C···N/N···C, and h) C···S/S···C.

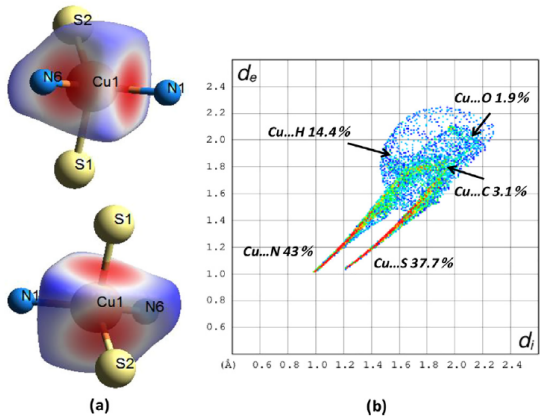

Fig. 9. a) Atomic Hirshfeld surface of Cu in complex 1 with the descriptor 'd_{norm}' mapped onto the surfaces and b) corresponding fingerprint plot for copper atom.

tacts (11.6% contribution), Fig. 8e, appear in the central region of the fingerprint plots with $d_e = d_i \approx 1.3$ Å, which indicates van der Waals interactions. The distribution of points in the $d_e = d_i \approx 1.7$ Å range in the fingerprint plot delineated into C···C contacts (Fig. 8f), indicates the existence of weak π–π stacking interactions between the pyridyl-(N1, C1–C5) and oxadiazole rings, which were reported in XRD studies. The π–π interaction are indicated by adjacent red and blue triangles in the shape-index map (Fig. 8c). The small contributions from other remaining interatomic contacts in complex **1** have negligible effect on the packing (Table S6). The large number of N···H/H···N, C···H/H···C, H···H and S···H/H···S, interactions suggest that van der Waals interactions and hydrogen bonding play dominant role in stabilizing the lattice of the complex structure, revealing also different packing modes.

Fig. 9a shows the Hirshfeld surfaces in the coordination geometry N_2S_2 about the copper atom of the copper polymeric complex that have been mapped to a normal surface. The dark red regions on the d_{norm} surface for Cu show the contact between N–Cu (the bond distance vary between 2.015 to 2.053 Å) and Cu–S (Cu–$S \approx$ 2.271 - 2.367 Å). Although the coordination covalent bonds with the sulphur and nitrogen atoms are dominant (Fig. 9b), there is weak areas of contact that can be attributed to H···Cu interactions. The Cu atom has up to 43% of the contacts from the N–Cu interaction on the Hirshfeld surface ($d_e + d_i \approx 2.0$ Å), 37.7% of the contacts from the S–Cu coordinates and the remaining 14.4% from H···Cu bonds. The HS of the metal centre relatively differentiates strong bonds weaker contacts taking place within the interaction sphere.

3.4. Magnetic study

The magnetic susceptibility of complex **1** has been measured under 0.5 T from 400 K to 2 K, to confirm the diamagnetic nature of the investigated copper complex. Indeed, the magnetization was found negative and nearly-temperature independent. The most prominent validation of Cu^{I} can be shown in Fig. 10, where M(H) at 300 K and 2 K are shown before and after corrections of the diamagnetism of the empty sample holder. The negative raw data return after correction to tiny magnetization values. At 2 K, the corrected M(H) shows a typical Brillouin-function evolution nearly saturated at 9T, Ms $\sim 10^{-3}$ μ_B/FU. It suggests the presence of a minor amount of Cu^{II}-side phase, in proportion 0.01% based on the $Cu^{2+}_{impurity}/Cu^{+}_{phase}$ ratio, well below the detection by XRD.

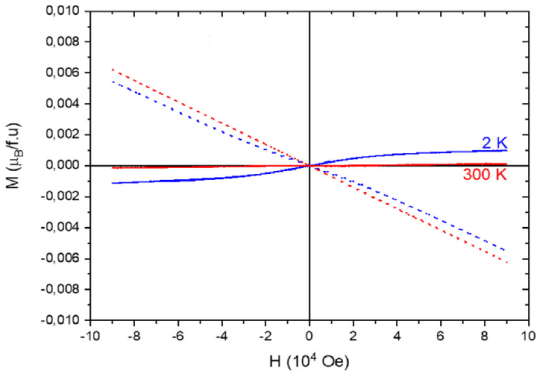

Fig. 10. Magnetization M(H) of complex 1 collected at 300 K (red) and 2 K (blue) before (dotted lines) and after (full-line) corrections of the sample-holder diamagnetism.

4. Conclusion

New Cu^{I} coordination polymer has been synthetized by means of self-assemblies of 2,5-bis(pyridin-4-yl)−1,3,4-oxadiazole (4-pox), thiocyanate ions, and Cu^{II} salt, and structurally characterized by X-ray diffraction analyses. The spectroscopic and thermal studies were also performed. The reduction of Cu^{II} to Cu^{I} in acetone solution leads to the formation of complex **1** which crystallizes in the monoclinic crystal system with space group $P21/n$. The obtained structure shows 1-D architecture of the title complex and is mainly stabilized by intermolecular hydrogen bonding, π–π stacking, and coordination bonds (N–Cu and S–Cu). Thermal decomposition study reveals that the investigated Cu^{I} coordination polymer is thermally stable up to 160 °C and the magnetic measurements show a diamagnetic behaviour.

Data availability

Data will be made available on request.

Credit author statement

Abdelhakim Laachir: Formal analysis, Methodology. **Ferdaousse Rhoufal**: Formal analysis, Methodology. **Salaheddine Guesmi:** Data curation, Conceptualization, Writing- Original draft preparation. **El Mostafa Ketatni:** Software, Validation. **Mohamed Saadi:** Formal analysis, Software. **Lahcen El Ammari:** Methodology, Software, Investigation. **Olivier Mentré:** Methodology, Software, Investigation. **Fouad Bentiss:** Conceptualization, Supervision, Writing- Reviewing and Editing.

Declaration of Competing Interest

The authors declare that they have no known competing financial interests or personal relationships that could have appeared to influence the work reported in this paper.

Acknowledgment

The authors thank the Faculty of Science, Mohammed V University in Rabat, Morocco for the X-ray measurements and the CUR CA2D of Chouaib Doukkali University (El Jadida Morocco) for its support. The European Regional Development Funds, CNRS, Nord Pas-de Calais Region, and Ministry of National Education, Higher Education and Research are acknowledged for funding the PPMS

system. We thank Laurence Claire Minaud for her magnetic experimental contribution.

Supplementary materials

Supplementary material associated with this article can be found, in the online version, at doi:10.1016/j.molstruc.2022.133790.

References

[1] X. Luo, R. Abazari, M. Tahir, W.K. Fan, A. Kumar, T. Kalhorizadeh, A.M. Kirillov, A.R. Amani Ghadim, J. Chen, Y. Zhou, Coord. Chem. Rev. 461 (2022) 214505.
[2] A.R. Woldu, Z. Huang, P. Zhao, L. Hu, D. Astruc, Coord. Chem. Rev. 454 (2022) 214340.
[3] Y. Zhou, R. Abazari, J. Chen, M. Tahir, A. Kumar, R.R. Ikreedeegh, E. Rani, H. Singh, A.M. Kirillov, Coord. Chem. Rev. 451 (2022) 214264.
[4] A.N. Bilyachenko, M.S. Dronova, A.L. Yalymov, F. Lamaty, X. Bantreil, J. Martinez, C. Bizer, L.S. Shul'pina, A.M. Korlyukov, D.E. Arkhipov, M.M. Levitsky, E.S. Shubina, A.M. Kirillov, G.B. Shul'pin, Chem. Eur. J. 21 (2015) 8758–8770.
[5] P.J. Figiel, A.M. Kirillov, M.F.C.G. da Silva, J. Lasri, A.J. Pombeiro, Dalton Trans 39 (2010) 9879–9888.
[6] A.M. Kirillov, M.V. Kirillova, A.J. Pombeiro, Adv. Inorg. Chem. 65 (2013) 1–31.
[7] N.Y. Li, Z.D. Jiang, Y.J. Wang, L.L. Liu, D. Liu, Inorg. Chem. 60 (2021) 17173–17177.
[8] F. Yang, N.Y. Li, Y. Ge, D. Liu, CrystEngComm 23 (2021) 2783–2787.
[9] N.Y. Li, J.M. Chen, X.Y. Tang, G.P. Zhang, D. Liu, Chem. Commun. 56 (2020) 1984–1987.
[10] A. Laachir, S. Guesmi, M. Saadi, L. El Ammari, O. Mentré, H. Vezin, S. Colis, F. Bentiss, J. Mol. Struct. 1123 (2016) 400–406.
[11] S. Pal, A.K. Barik, S. Gupta, A. Hazra, S.K. Kar, S.M. Peng, G.H. Lee, R.J. Butcher, M.S. El Fallah, J. Ribas, Inorg. Chem. 44 (2005) 3880–3889.
[12] A. Roth, J. Becher, C. Herrmann, H. Gorls, G. Vaughan, M. Reiher, D. Klemm, W. Plass, Inorg. Chem. 45 (2006) 10066–10076.
[13] C.X. Yu, K.Z. Wang, X.J. Li, D. Liu, L.F. Ma, L.L. Liu, Cryst. Growth. Des. 20 (2020) 5251–5260.
[14] L. Jaremko, A.M. Kirillov, P. Smolenski, A.J.L. Pombeiro, Cryst. Growth. Des. 9 (2009) 3006–3010.
[15] A. Laachir, F. Bentiss, S. Guesmi, M. Saadi, L. El Ammari, Acta. Cryst. E 69 (2013) m351–m352.
[16] A. Laachir, H. Zine, S. Guesmi, E.M. Ketatni, M. Saadi, L. El Ammari, O. Mentré, F. Bentiss, Polyhedron 209 (2021) 115494.
[17] M.M. Whittaker, D.P. Ballou, J.W. Whittaker, Biochemistry 37 (1998) 8426–8436.
[18] B.P. Branchaud, M.P. Montague-Smith, D.J. Kosman, F.R. McLaren, J. Am. Chem. Soc. 115 (1993) 798–800.
[19] R.M. Wachter, B.P. Branchaud, Biochim. Biophys. Acta. Protein. Struct. Mol. Enzymol. 1384 (1998) 43–54.
[20] S.L. Dhonnar, R.A. More, V.A. Adole, B.S. Jagdale, N.V. Sadgir, S.S. Chobe, J. Mol. Struct. 1253 (2022) 132216.
[21] R. Shingare, Y. Patil, J. Sangshetti, R. Patil, D. Rajani, B. Madje, Polycycl. Aromat. Compd. (2022) 1–13.
[22] S. Harisha, J. Keshavayya, B.K. Swamy, S.M. Prasanna, C.C. Viswanath, B.N. Ravi, J. Mol. Liq. 271 (2018) 976 Energy. Environ. Focus 983.
[23] A. Laachir, F. Rhoufal, S. Guesmi, E.M. Ketatni, L. Jouffret, E. Hlil, N. Sergent, S. Obbade, F. Bentiss, J. Mol. Struct. 1208 (2020) 127892.
[24] Z.L. Fang, J.G. He, Q.S. Zhang, Q.K. Zhang, X.Y. Wu, R.M. Yu, C.Z. Lu, Inorg. Chem. 50 (2011) 11403 Energy Environ. Focus 11411.
[25] G.L. Wen, G.G. Huang, S.S. Shi, C. Sun, Y. Yao, J.L. Zou, L.T. Wang, Y.Y. Sun, Energy. Environ. Focus. 5 (2016) 103–107.
[26] H. Lin, B. Mu, X. Wang, J. Coord. Chem. 64 (2011) 3465–3474.
[27] H. Zine, L.A. Rifai, M. Faize, F. Bentiss, S. Guesmi, A. Laachir, A. Smaili, K. Makroum, A. Sahibeb-Dine, T. Koussa, J. Agric. Food. Chem. 64 (2016) 2661–2667.
[28] A. Smaili, L.A. Rifai, S. Esserti, T. Koussa, F. Bentiss, S. Guesmi, A. Laachir, M. Faize, Pestic. Biochem. Physiol. 143 (2017) 26–32.
[29] F. Bentiss, M. Lagrenée, H. Vezin, J.P. Wignacourt, E.M. Holt, O. Mentrê, J. Phys. Chem. Solids 65 (2004) 701–705.
[30] H. Zine, L.A. Rifai, T. Koussa, F. Bentiss, S. Guesmi, A. Laachir, K. Makroum, M. Belfaiza, M. Faize, Pest Manag. Sci. 73 (2017) 188–197.
[31] Y.P. Prananto, A. Urbarsch, B. Moubaraki, K.S. Murray, D.R. Turner, G.B. Deacon, S.R. Batten, Aust. J. Chem. 70 (2017) 516–528.
[32] D. Pandey, S.S. Narvi, R. Kumar, S. Chaudhuri, Inorg. Chem. Commun. 130 (2021) 108736.
[33] F.A. Mautner, R.C. Fischer, K. Reichmann, E. Gullett, K. Ashkar, S.S. Massoud, J. Mol. Struct. 1175 (2019) 797–803.
[34] F.A. Mautner, C. Berger, R.C. Fischer, S.S. Massoud, R. Vicente, Polyhedron 141 (2018) 17–24.
[35] S.Q. Luo, Q. Wang, J. Quan, M. Yang, Y. Wang, X. Zhang, Z.N. Chen, Transit. Met. Chem. 46 (2021) 415–421.
[36] M.P. Davydova, I.A. Bauer, V.K. Brel, M.I. Rakhmanova, I.Y. Bagryanskaya, A.V. Artem'ev, Eur. J. Inorg. Chem. 2020 (2020) 695–703.
[37] H.J. Shin, S. Lee, C. Kim, K.S. Min, Inorg. Chim. Acta. (2022) 120877.
[38] F. Rhoufal, A. Laachir, S. Guesmi, L. Jouffret, N. Sergent, S. Obbade, M. Akkurt, F. Bentiss, ChemistrySelect 4 (2019) 7773–7783.
[39] A. Laachir, F. Rhoufal, S. Guesmi, E.M. Ketatni, L. Jouffret, N. Sergent, S. Obbade, F. Bentiss, J. Mol. Struct. 1208 (2020) 127892.
[40] A. Laachir, F. Bentiss, S. Guesmi, M. Saadi, L. El Ammari, Acta. Cryst. E. 72 (2016) 1176–1178.
[41] M. Du, H. Liu, X.H. Bu, J. Chem. Crystallogr. 32 (2002) 57–61.
[42] Y. Fang, H. Liu, M. Du, Y. Guo, X. Bu, J. Mol. Struct. 608 (2002) 229–233.
[43] M. Du, X.J. Zhao, J. Mol. Struct. 694 (2004) 235–240.
[44] F. Rhoufal, F. Bentiss, S. Guesmi, E.M. Ketatni, M. Saadi, L. El Ammari, Acta Cryst. E. 75 (2019) 1046–1050.
[45] G. Mahmoudi, A. Morsali, Cryst. Eng. Comm. 9 (2007) 1062–1072.
[46] H. Wang, M.-X. Li, M. Shao, Z.-X. Wang, J. Mol. Struct. 889 (2008) 154–159.
[47] Z.-L. Fang, J.-G. He, Q.-S. Zhang, Q.-K. Zhang, X.-Y. Wu, R.-M. Yu, C.-Z. Lu, Inorg. Chem. 50 (2011) 11403–11411.
[48] F. Bentiss, M. Lagrenée, J. Heterocycl. Chem. 36 (1999) 1029–1032.
[49] Bruker APEX3 (Version 5.054), SAINT (Version 6.36A), (2016).
[50] L. Krause, R. Herbst-Irmer, G.M. Sheldrick, D. Stalke, J. Appl. Cryst. 48 (2015) 3–10.
[51] G.M. Sheldrick, Acta Cryst. A 71 (2015) 3–8.
[52] G.M. Sheldrick, Acta Cryst. C 71 (2015) 3–8.
[53] L. Farrugia, J. Appl. Cryst. 45 (2012) 849–854.
[54] C.F. Macrae, I.J. Bruno, J.A. Chisholm, P.R. Edgington, P. McCabe, E. Pidcock, L. Rodriguez-Monge, R. Taylor, J. van de Streek, P.A. Wood, J. Appl. Cryst. 41 (2008) 466–470.
[55] J. Rodriguez-Carvajal, FULPROF. Version (July 2006).
[56] H.M. Rierveld, Acta Cryst. 22 (1967) 151–152.
[57] M.A. Spackman, D. Jayatilaka, CrystEngComm 11 (2009) 19–32.
[58] J.J. McKinnon, D. Jayatilaka, M.A. Spackman, Chem. Commun. (2007) 3814–3816.
[59] P.R. Spackman, M.J. Turner, J.J. McKinnon, S.K. Wolff, D.J. Grimwood, D. Jayatilaka, M.A. Spackman, J. Appl. Cryst. 54 (2021) 1006–1011.
[60] D. Jayatilaka, D.J. Grimwood, A. Lee, A. Lemay, A.J. Russel, C. Taylor, S.K. Wolff, P. Cassam-Chenai, A. Whitton, TONTO -a Sstem for Comput. Chem. (2005).
[61] J.V. Handy, G. Ayala, R.D. Pike, Inorg. Chim. Acta. 456 (2017) 64–75.
[62] D. Tudela, J. Chem. Educ. 70 (1993) 174.
[63] A. Laachir, F. Bentiss, S. Guesmi, M. Saadi, L. El Ammari, IUCrData 2 (2017) x170465.
[64] P. Gómez-Saiz, J. García-Tojal, F.J. Arnáiz, M.A. Maestro, L. Lezama, T. Rojo, Inorg. Chem. Commun. 6 (2003) 558–560.
[65] L. Martínez, N. Veiga, C. Bazzicalupi, A. Bianchi, F. Lloret, C. Kremer, R. Chiozzone, Polyhedron 208 (2021) 115406.
[66] C. Caglioti, A. Paoletti, E.P. Ricci, Nucl. Instrum. Methods 3 (1958) 223–228.